OPEN ACCESS
IOP Publishing
Journal of Optics
J. Opt. **26** (2024) 075201 (11pp)
https://doi.org/10.1088/2040-8986/ad52a2

Tripartite entanglement in a detuned non-degenerate optical parametric oscillator

Jun Guo[1,*], **Jianfeng Tian**[1] **and Hengxin Sun**[2]

[1] Department of Physics, Taiyuan Normal University, Jinzhong 030619, People's Republic of China
[2] State Key Laboratory of Quantum Optics and Quantum Optics Devices, Institute of Opto-Electronics, Shanxi University, Taiyuan 030006, People's Republic of China

E-mail: guojun@tynu.edu.cn

Received 13 November 2023, revised 3 May 2024
Accepted for publication 31 May 2024
Published 14 June 2024

Abstract

Continuous variable multipartite entanglement is an important resource in quantum optics and quantum information. Non-degenerate optical parametric oscillator (NOPO), generally working in a resonant regime, can generate high quality tripartite entanglement. However, the detuning in a real experiment is inevitable and sometimes necessary, for instance, in an optomechanical system. We calculate the tripartite entanglement from a detuned triply quasi-resonant NOPO. Unlike the previous literature using inseparability criterion, we use the positivity of partial transpose, a sufficient and necessary criterion, to characterize the tripartite entanglement with full inseparability generated from a detuned NOPO. We also consider the influence of the pump and signal/idler losses on the tripartite entanglement. The results show that, the tripartite entanglement could exist even with a large detuning of several times cavity linewidth, and may be better for a detuned regime than for the resonant one under some conditions. With a fixed non-zero loss which always exists in a real experiment, an appropriate value of non-zero detuning could lead to the best entanglement. What's more, unlike the bipartite entanglement, which exists both below and above threshold, the tripartite entanglement only occurs for a nonzero classical amplitude of signal/idler field. The jumping between the tripartite and bipartite entanglement could make the NOPO become a quantum state switch element, which promises a potential application on the multiparty quantum secret sharing.

Keywords: tripartite entanglement, optical parametric oscillator, detuned, the positivity of partial transpose

1. Introduction

Continuous variable (CV) entanglement is an important quantum resource in quantum communication, quantum computation and quantum precision measurement [1–3]. Especially, the multipartite entanglement, is the core to realize quantum computation and quantum network. Tripartite entanglement, with the least number of entangled multi-party, is of great significance. Tripartite entanglement can be generated by coupling squeezed beams on beam splitters [4], or directly through nonlinear processes such as optical parametric down-conversion [5–9], second harmonic generation [10–13] and atomic four-wave mixing [14, 15]. Unlike method with beam splitter mixing of the same-frequency modes, direct optical parametric oscillator (OPO) could generate multicolor multipartite entanglement, which has wider applications into quantum internet [16–18]. OPO proves to be

* Author to whom any correspondence should be addressed.

an effective device to generate high-quality entanglement because of its low loss and strong nonlinearity. Three-color tripartite (pump-signal-idler) entanglement can be directly generated by a nondegenerate OPO (NOPO) above threshold [5, 6]. Quadripartite Greenberger–Horne–Zeilinger (GHZ) entanglement [19] or cluster entanglement [20] were also experimentally realized in virtue of the spatial modes.

The OPO usually works in a resonant regime. The frequencies of signal/idler/pump fields are the same to the cavity frequency. The detuning is introduced if the frequency of at least one laser beam is not resonant in the cavity. The detuning should be avoided in a conventional experiment for entanglement generation due to its losses. However, the detuning is inevitable in a real experiment limited by the control precision of the cavity length. What's more, the detuning is required in some particular experiments. For a laser interferometer gravitational wave detector (GWD), the detuning of the signal recycling cavity greatly enhances the sensitivity at the optical spring frequency band [21, 22]. Adding an optical parametric amplifier further enhances the optical spring effect [23–25]. Recently, a detuned OPO is used to generate frequency-dependent squeezing which is required to achieve the GWD sensitivity beyond the standard quantum limit across the whole frequency band [26]. In the cavity optomechanics, the detuning is a feasible experimental parameter to control the optomechanical coupling strength [27–29].

The detuned OPO has been investigated in the literature [26, 30]. In the early days, people may focus its classical properties such as bistable or self-pulsing behaviour, which exhibits period doubling and chaos [31, 32]. Then the impact of detunings on the squeezing [33, 34] and bipartite entanglement [35] was reported. In recent years, multipartite entanglement from a detuned OPO is also reported. The tripartite entanglement remains with a large detuning [36]. The detuning of the signal field impacts tripartite entanglement more than that of pump field [37]. All of the above literature use the inseparability criterion to characterize tripartite entanglement. And few of them focus on the hysteresis properties of tripartite entanglement induced by the detunings in an NOPO.

In this article, we consider all of the detunings, say that of the signal, idler and pump fields of a triply quasi-resonant NOPO. The positivity of partial transpose (PPT) [38, 39], instead of the inseparability criterion [4] is used to characterize the full tripartite entanglement. PPT is a sufficient and necessary condition to verify multipartite entanglement for $1\times N$ partitions, rather than the only-sufficient inseparability criterion. The results show that, although the tripartite entanglement generally decreases with the detunings increasing, it still exists with large detunings. Under some conditions, the tripartite entanglement may be better for a detuned regime than the resonant regime. Unlike the bipartite entanglement from NOPO may exist both below and above threshold, the tripartite entanglement only occurs with a non-zero solution of down-converted classical amplitude. This is reasonable because it is the pump depletion which constructs the quantum correlation between the pump and down-converted fields and finally leads to tripartite entanglement. We also consider the influence of the losses of the pump field and signal/idler field. Without detunings, the tripartite entanglement deteriorates with increasing loss. However, with detunings, the best entanglement may occur with a nonzero loss, even with a large loss. Furthermore, the tripartite entanglement exhibits hysteresis property like the classical field acts. By adjusting the detunings and the pump amplitude, the NOPO could be regarded as a quantum state (more precisely tripartite entangled state) switch.

The paper is organized as follows. Section 2 gives the Langevin equation and its steady-state solution. Section 3 gives the quantum Langevin equation and its solution in the Fourier frequency. A brief introduction of criteria of tripartite entanglement for inseparability and PPT is given in section 4. The numerical simulation of tripartite entanglement with/without detunings is given in section 5. The loss effect on the entanglement is simulated in section 6. In the discussion of section 7, the quantum state control with detuned NOPO is discussed.

2. Theoretical model

We consider the theoretical model of type-II NOPO shown in figure 1. A second order nonlinear crystal with the nonlinear coefficient of $\chi^{(2)}$ is placed in a triangle cavity. The input pump field of a frequency ω_0 is down-converted into two fields of frequencies ω_1 and ω_2. The γ_i $(i=0,1,2)$ are the total loss parameters respectively of the pump, signal and idler fields. We consider the triply quasi-resonant case and define the detuning parameter as

$$\Delta_0=\frac{\omega_0-\omega_0^{'}}{\gamma_0/\tau},\ \Delta_1=\frac{\omega_1-\omega_1^{'}}{\gamma_1/\tau},\ \Delta_2=\frac{\omega_2-\omega_2^{'}}{\gamma_2/\tau}, \tag{1}$$

where $\omega_i^{'}(i=0,\,1,\,2)$ are the resonant frequencies respectively corresponding to the pump, signal and idler fields, τ the cavity round-trip time. Neglecting all of the intracavity losses, the loss parameters are related to the amplitude reflection (transmission) coefficients r_i (t_i) of the coupling mirrors through

$$r_i=1-\gamma_{b_i},\ t_i=\sqrt{2\gamma_{b_i}},\ i=0,1,2, \tag{2}$$

where γ_{b_i} are the one-pass loss parameters corresponding to the input-output mirrors.

The Langevin motional equations, which could be derived from the Heisenberg motional equations, considering intracavity losses, are given by

$$\tau\dot{\hat{a}}_0=-\gamma_0\left(1-i\Delta_0\right)\hat{a}_0-2\chi^{*}\hat{a}_1\hat{a}_2+\sqrt{2\gamma_{b_0}}\hat{a}_0^{in}+\sqrt{2\gamma_{c_0}}\hat{c}_0^{\mathrm{in}}, \tag{3a}$$

$$\tau\dot{\hat{a}}_1=-\gamma_1\left(1-i\Delta_1\right)\hat{a}_1+2\chi\hat{a}_2^{\dagger}\hat{a}_0+\sqrt{2\gamma_{b_1}}\hat{a}_1^{\mathrm{in}}+\sqrt{2\gamma_{c_1}}\hat{c}_1^{\mathrm{in}}, \tag{3b}$$

$$\tau\dot{\hat{a}}_2=-\gamma_2\left(1-i\Delta_2\right)\hat{a}_2+2\chi\hat{a}_1^{\dagger}\hat{a}_0+\sqrt{2\gamma_{b_2}}\hat{a}_2^{\mathrm{in}}+\sqrt{2\gamma_{c_2}}\hat{c}_2^{\mathrm{in}}, \tag{3c}$$

where $\hat{a}_i$ $(i=0,1,2)$ are the corresponding intracavity annihilation operators, χ the nonlinear coupling coefficient,

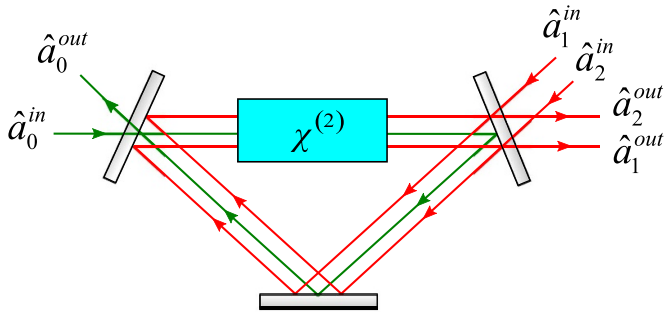

Figure 1. The theoretical model of non-degenerate optical parametric oscillator. $\hat{a}_i^{\rm in}$ $(i=0,1,2)$ are the annihilation operators of the incoming pump and signal fields, and $\hat{a}_i^{\rm out}$ $(i=0,1,2)$ the corresponding output fields.

γ_{c_i} the intracavity losses due to the absorption, surface scattering, and the total loss parameters $\gamma_i=\gamma_{b_i}+\gamma_{c_i}$. The $\hat{a}_i^{\rm in}$ $(i=0,1,2)$ are the annihilation operators of input fields. The $\hat{c}_i^{\rm in}$ $(i=0,1,2)$ are the annihilation operators of input vacuum fields from intracavity losses. For the convenience of numerical simulation, assuming $\gamma_{b_1}=\gamma_{b_2}=\gamma_b, \gamma_{c_1}=\gamma_{c_2}=\gamma_c$, we define the intracavity losses of pump and signal (idler) fields as

$$l_0=\frac{\gamma_{c_0}}{\gamma_{b_0}+\gamma_{c_0}} \tag{4}$$

and

$$l_1=l_2=\frac{\gamma_c}{\gamma_b+\gamma_c}. \tag{5}$$

Using the semiclassical approach, we have $\hat{a}_i=<\hat{a}_i>+\delta\hat{a}_i=\alpha_i+\delta\hat{a}_i$, where α_i and $\delta\hat{a}_i$ are the classical amplitudes and quantum fluctuations associated with the intracavity fields. Ignoring all of the fluctuations and intracavity losses, the equations of motion of the classical amplitudes are given by [33, 35]

$$\tau\dot{\alpha}_0=-\gamma_0\left(1-i\Delta_0\right)\alpha_0-2\chi^*\alpha_1\alpha_2+\sqrt{2\gamma_{b_0}}\alpha_0^{in}, \tag{6a}$$
$$\tau\dot{\alpha}_1=-\gamma_1\left(1-i\Delta_1\right)\alpha_1+2\chi\alpha_2^*\alpha_0, \tag{6b}$$
$$\tau\dot{\alpha}_2=-\gamma_2\left(1-i\Delta_2\right)\alpha_2+2\chi\alpha_1^*\alpha_0. \tag{6c}$$

The equations above could give the dynamical behavior of the cavity fields. However, to investigate the squeezing or entanglement generation, we focus on the steady-state results. Making the left side of the equation (6) be zero, the steady-state equations are given by [40]

$$\gamma_0\left(1-i\Delta_0\right)\alpha_0=-2\chi^*\alpha_1\alpha_2+\sqrt{2\gamma_{b_0}}\alpha_0^{\rm in}, \tag{7a}$$
$$\gamma_1\left(1-i\Delta_1\right)\alpha_1=2\chi\alpha_2^*\alpha_0, \tag{7b}$$
$$\gamma_2\left(1-i\Delta_2\right)\alpha_2=2\chi\alpha_1^*\alpha_0. \tag{7c}$$

Below the threshold, the gain of the down-converted fields is smaller than the loss, then the average amplitudes of the intracavity signal and idler fields are both zero, thus the steady-state solutions below threshold are given by

$$\alpha_1=\alpha_2=0,\ \alpha_0=\frac{\sqrt{2\gamma_{b_0}}\alpha_0^{\rm in}}{\gamma_0\left(1-i\Delta_0\right)}. \tag{8}$$

Above the threshold, the oscillation condition of triply resonant OPO requires the two detunings of down-converted fields are the same [40]

$$\Delta_1=\Delta_2=\Delta. \tag{9}$$

Solving equations (7), by multiplying the conjugate of the second by the third one, the pump threshold is given by

$$|\alpha_0^{\rm in}|_{\rm th}^2=\frac{\gamma_0^2\gamma_1\gamma_2}{8|\chi|^2\gamma_{b_0}}\left(1+\Delta^2\right)\left(1+\Delta_0^2\right). \tag{10}$$

We can see that the pump threshold increases not only with losses (including intracavity and output coupling losses of all the fields) increasing, but also with the detunings Δ and Δ_0 increasing. Then the pump parameter normalized to the pump threshold is given by

$$\sigma=\frac{|\alpha_0^{\rm in}|^2}{|\alpha_0^{\rm in}|_{\rm th}^2}. \tag{11}$$

Note that we normalize the pump intensity to the real pump threshold including the detunings, unlike [40] where the pump is normalized to the resonant threshold. This normalization makes it convenient to study the variation of entanglement with the pump intensity with the detunings.

Using equation (7), we yield an equation of intracavity signal field

$$\frac{\left(1-\Delta\Delta_0+\frac{4|\chi|^2|\alpha_1|^2}{\gamma_2\gamma_0}\right)^2+\left(\Delta+\Delta_0\right)^2}{\left(1+\Delta^2\right)\left(1+\Delta_0^2\right)}=\sigma. \tag{12}$$

Two cases are related to the solution of equation (12) as follows.

Case 1: $\Delta_0\Delta\leqslant 1$

When $\sigma\geqslant\sigma_{\rm th}=1$, the intracavity signal/idler intensity, $I_j^{\rm cav}=|\alpha_j|^2$, $(j=1,2)$, has one nonzero solution

$$I_j^{\rm cav}=\frac{\gamma_k\gamma_0}{4|\chi|^2}\left\{\left[\sigma\left(1+\Delta^2\right)\left(1+\Delta_0^2\right)-\left(\Delta_0+\Delta\right)^2\right]^{1/2}+\Delta_0\Delta-1\right\}, \tag{13}$$

where $j,k=1,2, j\neq k$. The OPO operates in a monostable regime, shown in figure 2(a). However, the solution will not be stable if two conditions as follows are simultaneously satisfied [32, 33],

$$\Delta\Delta_0<-\left(1+\frac{1+\Delta_0^2}{2\gamma'}\right), \tag{14a}$$
$$I_j^{\rm cav}>\frac{\left(1+\Delta_0^2\right)\left[1+\Delta_0^2+4\gamma'\left(1+\gamma'\right)\right]}{-2\left(1+\gamma'\right)^2\left[1+\Delta_0^2+2\gamma'\left(1+\Delta_0\Delta\right)\right]}, \tag{14b}$$

where we assume the two loss parameters of down-converted fields are the same, i.e. $\gamma_1=\gamma_2=\gamma$ for most cases in the following, $\gamma'=\gamma/\gamma_0$. This unstable region is plotted with dashed line in figure 2(a).

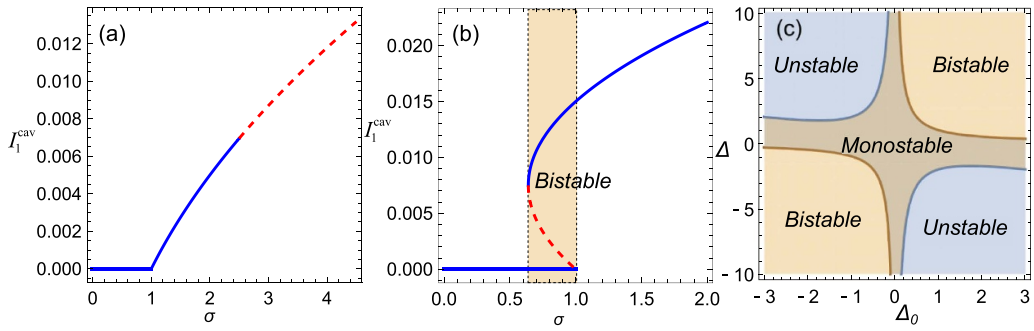

Figure 2. The normalized signal field intensity $I_1^{\rm cav}$ vs the normalized pump parameter σ: (a) monostable curves, where $\Delta_0 = 1, \Delta = -3, \gamma' = 1$; (b) bistable curves, where $\Delta_0 = 2, \Delta = 2, \gamma' = 1$. The blue solid lines denote stable solutions, the red dashed lines denote unstable solutions; (c) Region map of stability in the (Δ, Δ_0) plane with $\gamma' = 1$ denoted by monostable, bistable and unstable, respectively.

Case 2: $\Delta_0\Delta > 1$

When $\sigma_{\rm bis}^{\rm th} = \frac{(\Delta+\Delta_0)^2}{(1+\Delta^2)(1+\Delta_0^2)} < \sigma < \sigma^{\rm th} = 1$, three solutions are obtained, while only two of them are stable, so OPO may operate in a bistable regime, shown in figure 2(b). The $\sigma_{\rm bis}^{\rm th}$ is the bistable pump threshold. In this region, the two stable solutions of intracavity signal/idler intensity are given by

$$I_j^{\rm cav} = \frac{\gamma_k\gamma_0}{4|\chi|^2}\left\{\left[\sigma\left(1+\Delta^2\right)\left(1+\Delta_0^2\right) - \left(\Delta_0+\Delta\right)^2\right]^{1/2} + \Delta_0\Delta - 1\right\}, \tag{15a}$$

$$I_j^{\rm cav} = 0. \tag{15b}$$

Above threshold, $\sigma > 1$, the solutions are the same to equation (15*a*) and also to equation (13).

As analyzed above, OPO could operate in three regime, depending on the value of two detunings, Δ and Δ_0. In figure 2(c), the three regime is shown in the (Δ, Δ_0) plane.

Now we consider the phases of intracavity average fields. Beginning with equations (7), and assuming the phases of intracavity pump, signal and idler fields are respectively $\varphi_0, \varphi_1, \varphi_2$, i.e. $\alpha_0 = |\alpha_0|e^{i\varphi_0}$, $\alpha_1 = |\alpha_1|e^{i\varphi_1}$, $\alpha_2 = |\alpha_2|e^{i\varphi_2}$, then the steady-state equations become

$$\gamma_0\left(1 - i\Delta_0\right)|\alpha_0|e^{i\varphi_0} = -2\chi^*|\alpha_1||\alpha_2|e^{i(\varphi_1+\varphi_2)} + \sqrt{2\gamma_{b_0}}\alpha_0^{in}, \tag{16a}$$

$$\gamma_1\left(1 - i\Delta\right)|\alpha_1|e^{i\varphi_1} = 2\chi|\alpha_2||\alpha_0|e^{i(\varphi_0-\varphi_2)}, \tag{16b}$$

$$\gamma_2\left(1 - i\Delta\right)|\alpha_2|e^{i\varphi_2} = 2\chi|\alpha_1||\alpha_0|e^{i(\varphi_0-\varphi_1)}. \tag{16c}$$

Assuming two down-converted fields have the same phase and the same intensity, i.e. $\varphi_1 = \varphi_2 = \varphi$ and $|\alpha_1| = |\alpha_2| = |\alpha|$, then the steady-state solution above threshold in the monostable regime is given by

$$e^{2i\varphi} = \frac{2\chi\sqrt{2\gamma_{b_0}}\alpha_0^{\rm in}}{\gamma_0\gamma_1\left(1 - i\Delta_0\right)\left(1 - i\Delta\right) + 4|\chi|^2|\alpha|^2}, \tag{17a}$$

$$\alpha_0 = |\alpha_0|e^{i\varphi_0} = \frac{\gamma_1\left(1 - i\Delta\right)}{2\chi}e^{2i\varphi}, \tag{17b}$$

$$\alpha_1 = \alpha_2 = |\alpha|e^{i\varphi}, \tag{17c}$$

$$|\alpha| = \sqrt{\frac{\gamma_1\gamma_0}{4|\chi|^2}\left\{\left[\sigma\left(1+\Delta^2\right)\left(1+\Delta_0^2\right) - \left(\Delta_0+\Delta\right)^2\right]^{1/2} + \Delta_0\Delta - 1\right\}}. \tag{17d}$$

In the bistable regime, the nonzero steady-state solution is the same to that of monostable one, i.e. equations (17). This solution will be used in the following entanglement analysis.

3. Quantum Langevin equations and solutions

Using the semiclassical approaches and only considering the quantum fluctuation operators of equations (3), the quantum Langevin equations are given by

$$\tau\delta\dot{\hat{a}}_0 = -\gamma_0\left(1 - i\,\Delta_0\right)\delta\hat{a}_0 - 2\chi^*\left(\alpha_2\delta\hat{a}_1 + \alpha_1\delta\hat{a}_2\right) + \sqrt{2\gamma_{b_0}}\delta\hat{a}_0^{\rm in} + \sqrt{2\gamma_{c_0}}\hat{c}_0^{\rm in}, \tag{18a}$$

$$\tau\delta\dot{\hat{a}}_1 = -\gamma_1\left(1 - i\,\Delta_1\right)\delta\hat{a}_1 + 2\chi\left(\alpha_2^*\delta\hat{a}_0 + \alpha_0\delta\hat{a}_2^\dagger\right) + \sqrt{2\gamma_{b_1}}\delta\hat{a}_1^{\rm in} + \sqrt{2\gamma_{c_1}}\hat{c}_1^{\rm in}, \tag{18b}$$

$$\tau\delta\dot{\hat{a}}_2 = -\gamma_2\left(1 - i\,\Delta_2\right)\delta\hat{a}_2 + 2\chi\left(\alpha_1^*\delta\hat{a}_0 + \alpha_0\delta\hat{a}_1^\dagger\right) + \sqrt{2\gamma_{b_2}}\delta\hat{a}_2^{\rm in} + \sqrt{2\gamma_{c_2}}\hat{c}_2^{\rm in}. \tag{18c}$$

Introducing the quadrature amplitude and phase operators $\hat{X}=\hat{a}+\hat{a}^{\dagger}$ and $\hat{Y}=(\hat{a}-\hat{a}^{\dagger})/i$, we can write equations (18) in the matrix form as

$$\dot{f}(t)=Af(t)+\eta(t), \tag{19}$$

where $f(t)=(\delta\hat{X}_0,\delta\hat{Y}_0,\delta\hat{X}_1,\delta\hat{Y}_1,\delta\hat{X}_2,\delta\hat{Y}_2)^T$ is the transpose of the vector associated to the quadrature operators. The drift matrix A is written as

$$\frac{1}{\tau}\begin{pmatrix} -\gamma_0 & -\gamma_0\Delta_0 & -2\chi\,\mathrm{Re}(\alpha_2) & 2\chi\,\mathrm{Im}(\alpha_2) & -2\chi\,\mathrm{Re}(\alpha_1) & 2\chi\,\mathrm{Im}(\alpha_1)\\ \gamma_0\Delta_0 & -\gamma_0 & -2\chi\,\mathrm{Im}(\alpha_2) & -2\chi\,\mathrm{Re}(\alpha_2) & -2\chi\,\mathrm{Im}(\alpha_1) & -2\chi\,\mathrm{Re}(\alpha_1)\\ 2\chi\,\mathrm{Re}(\alpha_2) & 2\chi\,\mathrm{Im}(\alpha_2) & -\gamma_1 & -\gamma_1\Delta_1 & 2\chi\,\mathrm{Re}(\alpha_0) & 2\chi\,\mathrm{Im}(\alpha_0)\\ -2\chi\,\mathrm{Im}(\alpha_2) & 2\chi\,\mathrm{Re}(\alpha_2) & \gamma_1\Delta_1 & -\gamma_1 & 2\chi\,\mathrm{Im}(\alpha_0) & -2\chi\,\mathrm{Re}(\alpha_0)\\ 2\chi\,\mathrm{Re}(\alpha_1) & 2\chi\,\mathrm{Im}(\alpha_1) & 2\chi\,\mathrm{Re}(\alpha_0) & 2\chi\,\mathrm{Im}(\alpha_0) & -\gamma_2 & -\gamma_2\Delta_2\\ -2\chi\,\mathrm{Im}(\alpha_1) & 2\chi\,\mathrm{Re}(\alpha_1) & 2\chi\,\mathrm{Im}(\alpha_0) & -2\chi\,\mathrm{Re}(\alpha_0) & \gamma_2\Delta_2 & -\gamma_2 \end{pmatrix}, \tag{20}$$

where Re() and Im() respectively denote the real and imaginary part of the complex amplitude of the fields. For simplicity, the χ is assumed to be real, i.e. the phase-matching condition is fulfilled [40]. The diffusion matrix is given by

$$\begin{aligned}\eta(t)=&\frac{1}{\tau}\Big(\sqrt{2\gamma_{b_0}}\delta\hat{X}^{\mathrm{in}}_{a_0}+\sqrt{2\gamma_{c_0}}\delta\hat{X}^{\mathrm{in}}_{c_0},\sqrt{2\gamma_{b_0}}\delta\hat{Y}^{\mathrm{in}}_{a_0}+\sqrt{2\gamma_{c_0}}\delta\hat{Y}^{\mathrm{in}}_{c_0},\\ &\sqrt{2\gamma_{b_1}}\delta\hat{X}^{\mathrm{in}}_{a_1}+\sqrt{2\gamma_{c_1}}\delta\hat{X}^{\mathrm{in}}_{c_1},\sqrt{2\gamma_{b_1}}\delta\hat{Y}^{\mathrm{in}}_{a_1}+\sqrt{2\gamma_{c_1}}\delta\hat{Y}^{\mathrm{in}}_{c_1},\\ &\sqrt{2\gamma_{b_2}}\delta\hat{X}^{\mathrm{in}}_{a_2}+\sqrt{2\gamma_{c_2}}\delta\hat{X}^{\mathrm{in}}_{c_2},\sqrt{2\gamma_{b_2}}\delta\hat{Y}^{\mathrm{in}}_{a_2}+\sqrt{2\gamma_{c_2}}\delta\hat{Y}^{\mathrm{in}}_{c_2}\Big)^T\\ \equiv&\frac{1}{\tau}\left(Bf^{\mathrm{in}}_a+Cf^{\mathrm{in}}_c\right),\end{aligned} \tag{21}$$

with two coefficient-related diagonal matrices

$$B=\mathrm{diag}\left(\sqrt{2\gamma_{b_0}},\sqrt{2\gamma_{b_0}},\sqrt{2\gamma_{b_1}},\sqrt{2\gamma_{b_1}},\sqrt{2\gamma_{b_2}},\sqrt{2\gamma_{b_2}}\right), \tag{22a}$$

$$C=\mathrm{diag}\left(\sqrt{2\gamma_{c_0}},\sqrt{2\gamma_{c_0}},\sqrt{2\gamma_{c_1}},\sqrt{2\gamma_{c_1}},\sqrt{2\gamma_{c_2}},\sqrt{2\gamma_{c_2}}\right), \tag{22b}$$

and f^{in}_a, f^{in}_c are respectively the input vectors of vacuum fluctuations through the coupling mirrors and the intracavity losses.

By Fourier transform of equation (19) with $f(\omega)=\int_{-\infty}^{+\infty}f(t)e^{-i\omega t}\mathrm{d}t$ and using equation (21), we have

$$\begin{aligned}i\omega f(\omega)&=Af(\omega)+\eta(\omega)\\ &=Af(\omega)+\frac{1}{\tau}\left(Bf^{\mathrm{in}}_a(\omega)+Cf^{\mathrm{in}}_c(\omega)\right),\end{aligned} \tag{23}$$

where $f(\omega)$ and $\eta(\omega)$ are respectively the Fourier transform of $f(t)$ and $\eta(t)$, $f^{\mathrm{in}}_a(\omega)=(\delta\hat{X}^{\mathrm{in}}_{a_0}(\omega),\delta\hat{Y}^{\mathrm{in}}_{a_0}(\omega),\delta\hat{X}^{\mathrm{in}}_{a_1}(\omega),\delta\hat{Y}^{\mathrm{in}}_{a_1}(\omega),\delta\hat{X}^{\mathrm{in}}_{a_2}(\omega),\delta\hat{Y}^{\mathrm{in}}_{a_2}(\omega))^T$, and $f^{\mathrm{in}}_c(\omega)$ has a similar form with $f^{\mathrm{in}}_a(\omega)$. Using the input–output relation of the cavity of $\hat{a}^{\mathrm{out}}=\sqrt{2\gamma}\hat{a}-\hat{a}^{\mathrm{in}}$ [41], we have

$$f^{\mathrm{out}}(\omega)=Bf(\omega)-f^{\mathrm{in}}_a(\omega), \tag{24}$$

with $f^{\mathrm{out}}(\omega)=(\delta\hat{X}^{\mathrm{out}}_{a_0}(\omega),\delta\hat{Y}^{\mathrm{out}}_{a_0}(\omega),\delta\hat{X}^{\mathrm{out}}_{a_1}(\omega),\delta\hat{Y}^{\mathrm{out}}_{a_1}(\omega),\delta\hat{X}^{\mathrm{out}}_{a_2}(\omega),\delta\hat{Y}^{\mathrm{out}}_{a_2}(\omega))^T$.

Solving equations (23) and (24), we have

$$\begin{aligned}f^{\mathrm{out}}(\omega)=&\left[\frac{1}{\tau}B(i\omega I-A)^{-1}B-I\right]f^{\mathrm{in}}_a(\omega)\\ &+\frac{1}{\tau}B(i\omega I-A)^{-1}Cf^{\mathrm{in}}_c(\omega),\end{aligned} \tag{25}$$

where I is the identity matrix. For convenience, the analyzing frequency normalized to the linewidth of the fundamental mode, $\Omega=\omega/(\gamma_1/\tau)$, is used in the following.

4. Criteria for characterizing tripartite entanglement

There are two frequently used criteria to characterize CV entanglement. The inseparability criterion developed by Loock and Furusawa [4] is more feasible in experiment. With the operators of the output fields of OPO, the inseparability criterion is written as

$$\left\langle\delta^2\left(\hat{X}_1-\hat{X}_2\right)\right\rangle+\left\langle\delta^2\left(\hat{Y}_1+\hat{Y}_2-g_1\hat{Y}_0\right)\right\rangle\geqslant 4, \tag{26a}$$

$$\left\langle\delta^2\left(\hat{X}_0+\hat{X}_1\right)\right\rangle+\left\langle\delta^2\left(\hat{Y}_1+g_2\hat{Y}_2-\hat{Y}_0\right)\right\rangle\geqslant 4, \tag{26b}$$

$$\left\langle\delta^2\left(\hat{X}_0+\hat{X}_2\right)\right\rangle+\left\langle\delta^2\left(g_3\hat{Y}_1+\hat{Y}_2-\hat{Y}_0\right)\right\rangle\geqslant 4, \tag{26c}$$

where the $g_i\,(i=0,1,2)$ are the gain factors which are chosen to minimize the variances on the left side of the inequalities. The tripartite entanglement exists, if any two of the three inequalities are violated. However, this is a sufficient condition for tripartite entanglement, rather than necessary [4].

The positive partial transposition (PPT) [38] is another criterion to characterize CV entanglement. An n-mode Gaussian state could be partitioned into two parts with $n_A+n_B=n$. According to PPT, if one party, say n_B, is separable from the rest (n_A), the full density matrix remains positive under partial transpose with respect to the party (n_B). This criterion is necessary and sufficient for $1\times N$ partitions of the state to verify multipartite entanglement, where 1 and N are the number of the modes of the first and second subsystem [42]. For three-mode system, three partitions of 1×2 should be tested. The positivity is checked by verifying the symplectic eigenvalues of the partially transposed covariance matrix. The state is separable if

and only if all of the symplectic eigenvalues are greater than or equal to 1. As we know, bipartite entanglement is simple on the level of 'separable or entangled'. In contrary, the multipartite entanglement may be fully separable, partially separable and fully inseparable [43]. Even the partially separable state itself may have different types, which makes the characterization of multipartite entanglement quite complex. Here we choose fully inseparable criterion. That is, full tripartite entanglement exists if and only if all of the smallest symplectic eigenvalues of the partially transposed covariance matrix corresponding to each partition of the three modes are smaller than 1 [6].

We use $\hat{f}=(\delta\hat{X}_0,\delta\hat{Y}_0,\delta\hat{X}_1,\delta\hat{Y}_1,\delta\hat{X}_2,\delta\hat{Y}_2)^T$ as the fluctuation operator vector of output fields. The canonical commutation relations between any two operators are expressed in the symplectic form as [39]

$$\left[\hat{f}_i,\hat{f}_j\right]=2i\mathbf{\Omega}_{ij},\ \mathbf{\Omega}\quad=\begin{pmatrix}J&0&0\\0&J&0\\0&0&J\end{pmatrix},J=\begin{pmatrix}0&1\\-1&0\end{pmatrix}. \tag{27}$$

The PPT employs covariance matrix $\boldsymbol{V}$ of the output fields according to its matrix elements

$$V_{ij}=\frac{1}{2}\langle\hat{f}_i\hat{f}_j+\hat{f}_j\hat{f}_i\rangle-\langle\hat{f}_i\rangle\langle\hat{f}_j\rangle, \tag{28}$$

where the square of the fluctuations is what we are interested into, the average part is set to be zero, i.e. $\langle\hat{f}_i\rangle=0$.

The partial transpose of the covariance matrix is given by

$$\tilde{\boldsymbol{V}}=\Lambda\boldsymbol{V}\Lambda, \tag{29}$$

where Λ could be one of the diagonal matrices: $\mathrm{diag}(1,1,1,-1,1,-1)$, $\mathrm{diag}(1,-1,1,1,1,-1)$ and $\mathrm{diag}(1,-1,1,-1,1,1)$, which are in fact the phase space mirror reflections of the Wigner distribution with respect to any two of the three output fields of OPO. The symplectic eigenvalue of the covariance matrix $\tilde{\boldsymbol{V}}$ can be computed as the absolute value of eigenvalues of matrix $i\mathbf{\Omega}\tilde{\boldsymbol{V}}$. In the following we use s_0, s_1, s_2 to denote the smallest symplectic eigenvalue corresponding to the partial transposes with respect to the pump, signal and idler fields. The tripartite entanglement is numerically characterized by PPT criterion in the next section.

5. Numerical simulation

Take the results of equation (24) into equation (29), the matrix $i\mathbf{\Omega}\tilde{\boldsymbol{V}}$ and its eigenvalue is obtained. The following parameters are used, unless specified: $\gamma_1=\gamma_2=0.02$, $\gamma_0=0.1$, $\sigma=1.5$, $\Omega=0.1$.

5.1. Tripartite entanglement without detunings

Firstly, we give the tripartite entanglement without detunings. Figure 3 gives the smallest symplectic eigenvalues as a function of the normalized pump parameter for various normalized analyzing frequencies. The tripartite entanglement exists with selected parameters, as all of the smallest symplectic eigenvalues are smaller than 1. Note that $s_1=s_2$ because the signal and idler fields are interchangeable. For the same parameters, s_1, s_2 are always smaller than s_0, due to the signal (or idler) field exhibits stronger correlation to the whole system than the pump field [5, 6, 8, 37, 44]. The increased analyzing frequency leads to larger symplectic eigenvalues, hence decreases entanglement. Furthermore, s_0 with near-threshold pump are very sensitive to the increasing analyzing frequency and becomes larger quickly. However, s_0 with the far-threshold pump changes little. Then an optimal pump intensity is needed to obtain the best entanglement. The symplectic eigenvalues versus analyzing frequency are plotted in figure 4. The eigenvalues across a large scope of analyzing frequency Ω from 0 to 5 are given, showing a monotonic increasing with Ω. Even so, the tripartite entanglement still exists.

5.2. Tripartite entanglement with detunings

As analyzed in section 2, with detuning, the OPO may work in several regimes in terms of stable, bistable and unstable states, depending on the values of the two detunings, Δ_0, Δ, and/or the pump parameter σ (also see figure 2). Here we just consider the stable and bistable states.

By comparing equation (13) of *Case 1* with $\Delta\Delta_0\leqslant 1$ and equation (15*a*) of *Case 2* with $\Delta\Delta_0>1$, we find they have the same steady-state solution of intracavity signal/idler field. Therefore, the non-zero solution and the tripartite entanglement degree are continuous when crossing $\Delta\Delta_0=1$. However, the zero solution in the bistable region could not exhibit tripartite entanglement [5, 6]. This is shown in figure 5.

For the non-zero solution, the smallest symplectic eigenvalues as a function of the detunings are shown in figure 6. The dependence of eigenvalues on the two detunings are almost the same. The s_0 is much larger than s_1, s_2. For $\Delta_0=0$, the s_0 has a minimum at $\Delta=0$, while for $\Delta_0=1$, the s_0 has a minimum at $\Delta\sim 0.3$. Roughly speaking, the detunings decrease the tripartite entanglement, which is consistent with the literature for squeezing and bipartite entanglement [33, 37, 45, 46].

6. Loss effect on tripartite entanglement

6.1. Loss without detunings

We first plot the effect of losses of pump l_0 and signal (idler) $l_1=l_2$ on tripartite entanglement, shown in figure 7. With increasing losses, all of the symplectic values become larger and thus indicating less tripartite entanglement. By comparison, the s_1, s_2 are much more sensitive to the signal/idler loss than to the pump loss. What's more, the s_0 becomes larger with a pump parameter near threshold. A relatively larger pump could ease the requirement to the losses, which is consistent to the experimental results reported in [6].

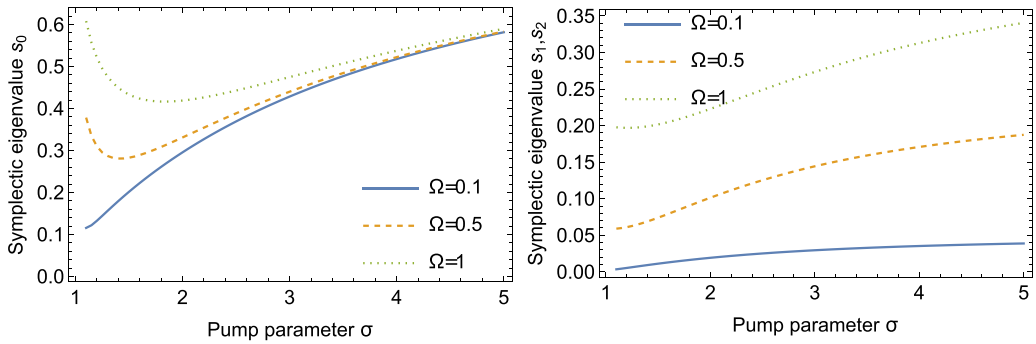

Figure 3. The smallest symplectic eigenvalues s_0 (left) and s_1, s_2 (right) as a function of the normalized pump parameter without detunings, for various normalized analyzing frequencies of $\Omega = 0.1, 0.5, 1$. s_1, s_2 are always smaller than s_0. A higher analyzing frequency may lead to an increasing s_0 near threshold, rather than that far from threshold. This induces an optimal pump intensity (not at threshold) for observing tripartite entanglement.

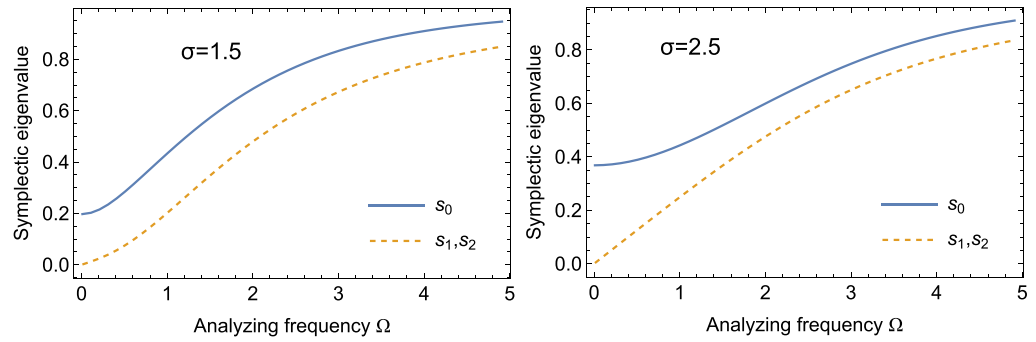

Figure 4. The smallest symplectic eigenvalues as a function of the normalized analyzing frequency without detunings, for various pump parameters of $\sigma = 1.5$ (left) and $\sigma = 2.5$ (right).

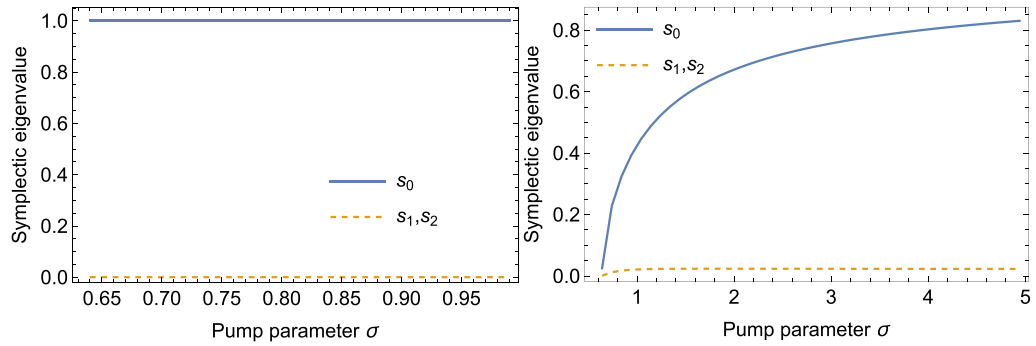

Figure 5. The smallest symplectic eigenvalues as a function of the pump parameter for the zero solution (left) and nonzero solution (right) of intracavity signal/idler intensity, with other fixed parameters: $\Delta = 2$, $\Delta_0 = 2$, $\sigma_{\rm bis} = 0.64$, $\Omega = 0.1$. The smallest symplectic eigenvalues above threshold ($\sigma > 1$) are also plotted. Obviously, no tripartite entanglement exists for zero solution of $|\alpha_{1,2}|$. Tripartite entanglement exists for nonzero solution of $|\alpha_{1,2}|$, and becomes stronger with increasing pump parameter from bistable threshold to that above threshold.

6.2. Loss with detunings

As shown in figure 6, the dependences of symplectic eigenvalues on the two detunings, say Δ and Δ_0, are very similar. Thus, for simplicity, we focus on the Δ dependence, while with fixed $\Delta_0 = 0$.

The symplectic eigenvalues as a function of signal/idler detunings are plotted in figure 8, with various values of pump loss, signal/idler loss, pump parameter and analyzing frequency. We could find a surprising phenomenon that the tripartite entanglement does not monotonously deteriorate with the detuning increasing. In the contrary, with large losses, there are two symmetric detuning values around zero to get the best tripartite entanglement, which could be obviously seen in figures 8(a)–(d) with $l_0 = 0.75$ or $l_1 = 0.75$. What's more, the best entanglement with great loss is better than that without any loss. Decreasing pump power from $\sigma = 1.5$ to $\sigma = 1.1$, greatly enhances the entanglement without any loss, see figures 8(e) and (f). Decreasing analyzing frequency, could enhance the extreme value of entanglement across the detuning, but not change the shape of oscillation, see figures 8(g) and (h).

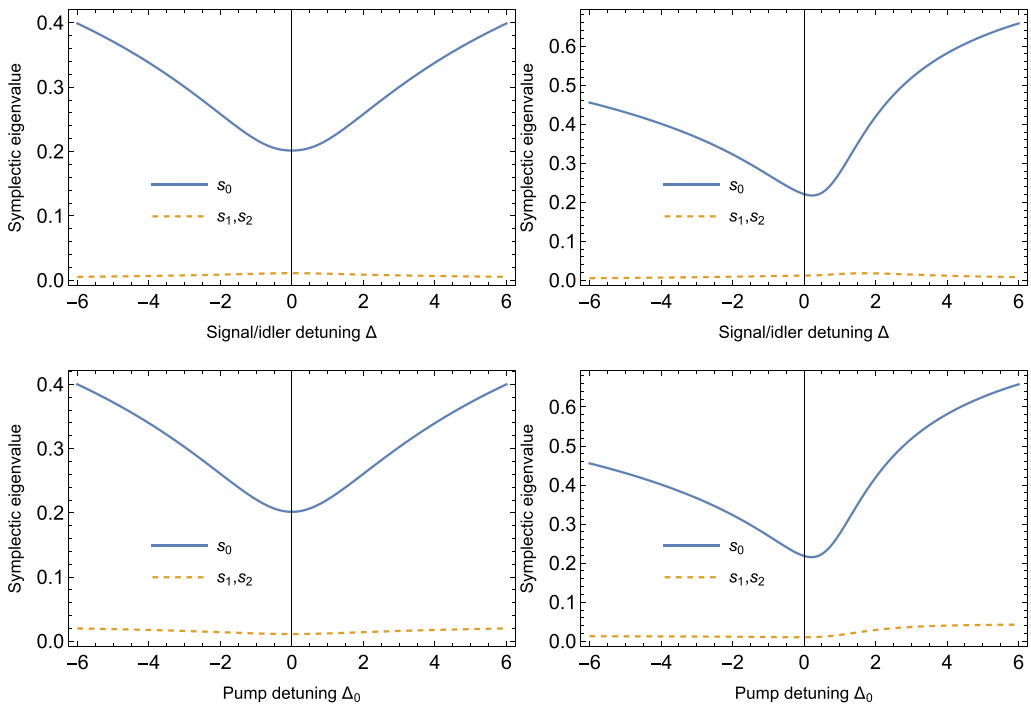

Figure 6. Effect of detunings on the tripartite entanglement with symplectic eigenvalue versus Δ (top left, with fixed $\Delta_0 = 0$ and top right, with fixed $\Delta_0 = 1$) and Δ_0 (bottom left, with fixed $\Delta = 0$ and bottom right, with fixed $\Delta = 1$), respectively.

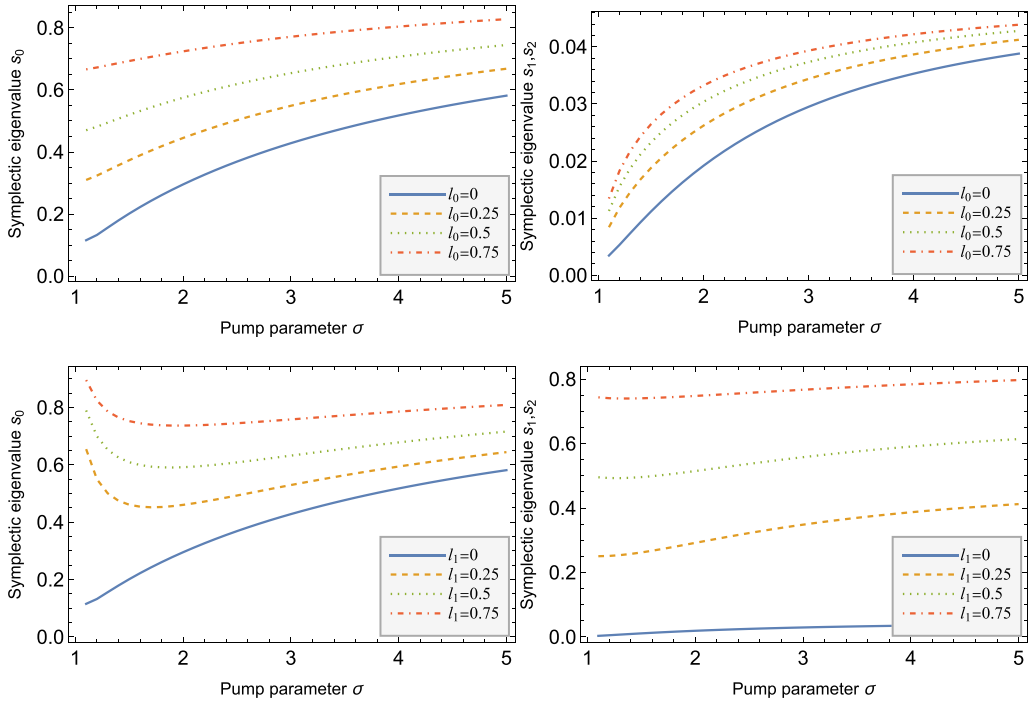

Figure 7. Effect of losses on the tripartite entanglement with symplectic eigenvalue versus pump parameter with pump loss (top) and signal/idler loss (bottom), respectively.

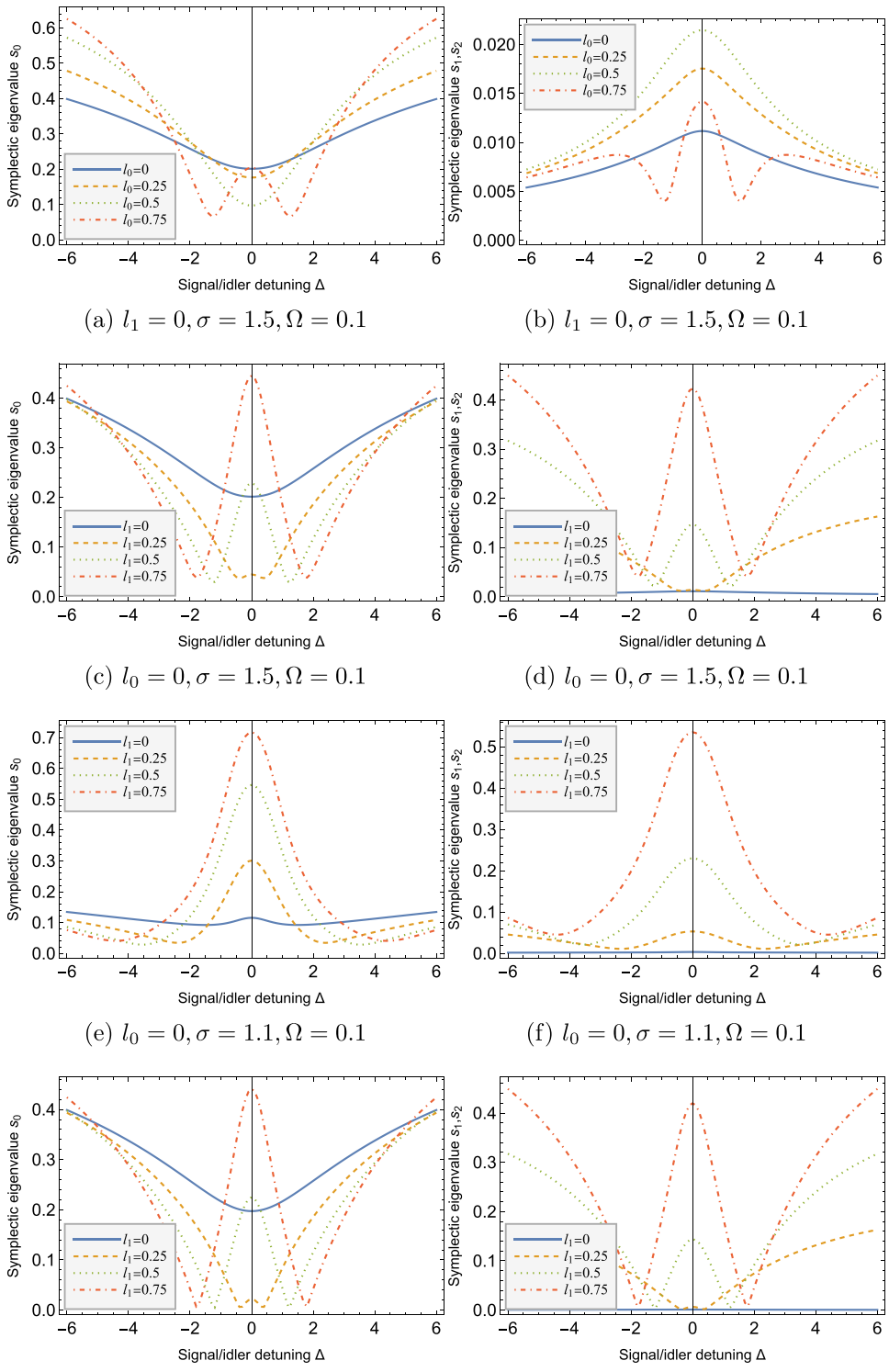

(a) $l_1 = 0, \sigma = 1.5, \Omega = 0.1$ (b) $l_1 = 0, \sigma = 1.5, \Omega = 0.1$

(c) $l_0 = 0, \sigma = 1.5, \Omega = 0.1$ (d) $l_0 = 0, \sigma = 1.5, \Omega = 0.1$

(e) $l_0 = 0, \sigma = 1.1, \Omega = 0.1$ (f) $l_0 = 0, \sigma = 1.1, \Omega = 0.1$

(g) $l_0 = 0, \sigma = 1.5, \Omega = 0.01$ (h) $l_0 = 0, \sigma = 1.5, \Omega = 0.01$

Figure 8. Effect of pump loss (a)–(b), signal/idler loss (c)–(d), pump parameter(e)–(f) and analyzing frequency (g)–(h) on the symplectic eigenvalues. All the other subfigures should be compared with (c)–(d), which use initial parameters.

7. Discussions

In this paper, we numerically analyze the effect of detunings on the tripartite entanglement generated from an OPO. We find with a very large loss of signal/idler, an appropriate selection of detunings could retrieve a high-quality tripartite entanglement. It seems that detunings could compensate some loss to obtain a good entanglement. However, the physics behind this is still an open question. To our best knowledge, most of the works in the literature discuss more on the numerical results

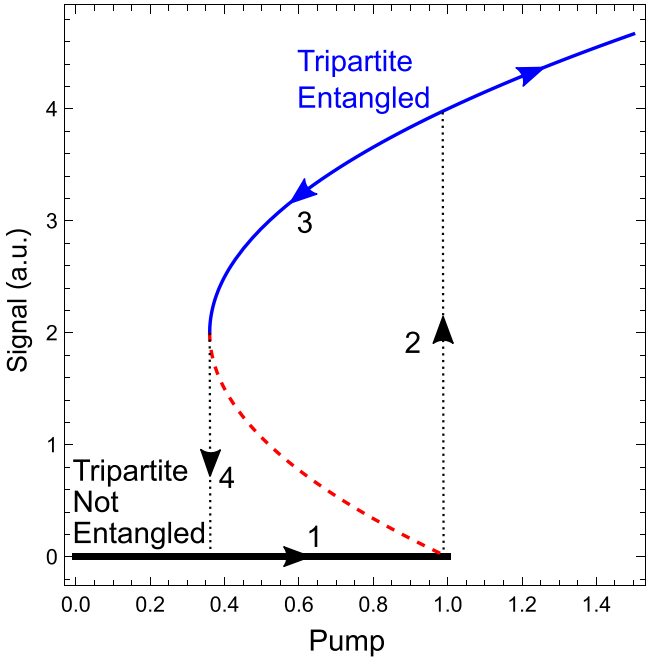

Figure 9. Tripartite entanglement control with pump intensity in a detuned OPO. The thick black line indicates the zero solution of signal/idler fields without tripartite entanglement. The blue line denotes the nonzero solution of signal/idler fields with tripartite entanglement. If we increase the pump, OPO may start from the *path 1* until it arrives at the threshold. Continuous increasing of pump makes OPO abruptly jump onto the blue line along *path 2* and get tripartite entanglement at threshold. If we decrease the pump from a point above threshold, OPO may goes into *path 3* until it arrives at bistable threshold. And then OPO jumps down to the black line along *path 4* and loses tripartite entanglement simultaneously. In this way, the tripartite entanglement is effectively controlled by the pump intensity operation. Note that this is different from bipartite entanglement which exists for both zero and nonzero solution.

of detunings, not on the physics behind the influence of detunings on the entanglement. Of course, the effect of detunings on the steady-state field strength is evident, but on the quantum correlation.

On the other hand, the detuned NOPO exhibits optical bistability, causing an optical hysteresis from the point of view of classical optical amplitude. The classical amplitude may be related to the quantum correlation such as quadrature squeezing and entanglement. As derived in the literature [33, 37, 45, 46], the bipartite entanglement exists both below and above threshold, thereby not exhibiting hysteresis. However, the tripartite entanglement does exhibit hysteresis as proved in the preceding text. The clearer demonstration of this hysteresis is shown in figure 9. The *tripartite not entangled* state below threshold would jump into the *tripartite entangled* state with increasing pump across threshold. The *tripartite entangled* state would not vanish abruptly when decreasing pump across threshold. In stead, it will keep for a while until the pump is reduced to the bistable threshold. What's more, as shown in figure 8, the best tripartite entanglement occurs in the bistable region. The variation of changing from non-entanglement to entanglement is very sharp (not continuous). This change could be regarded as *binary*. In this way, the tripartite entanglement could be controlled in a binary form by changing the pump. The NOPO could be regarded as a quantum state switch element, which has some similarity to the classical optical transistor behavior [47]. Note that, for a resonant NOPO, the binary state change is similar, while this hysteresis property is missing, thus it could not exhibit the transistor effect.

8. Conclusions

We calculate the tripartite entanglement among the signal, idler and pump fields from a detuned type-II OPO. Based on the PPT criterion (full inseparability), the tripartite entanglement depends on several parameters including losses, pump strength and analyzing frequency. With detunings, even a large intracavity loss could still guarantee a high-quality tripartite entanglement. Unlike bipartite entanglement which exists both below and above pump threshold, tripartite entanglement only exists for the down-converted nonzero solutions. With detunings, the best tripartite entanglement occurs in the bistable region. Similar to the down-converted classical field, the tripartite quantum entanglement also exhibits hysterical property. This property may make a detuned NOPO a quantum state controller such as a switch element.

Data availability statement

All data that support the findings of this study are included within the article (and any supplementary files).

Acknowledgments

This work is supported by National Natural Science Foundation of China (Grant No. 12004277), Scientific and Technological Innovation Programs of Higher Education Institutions in Shanxi (Grant No. 2020L0506), Shanxi Scholarship Council of China (Grant No. 2021-005), Natural Science Foundation of Shanxi Province (Grant No. 201901D111293) and Shanxi 1331 Project.

Conflict of interest

The authors declare no conflicts of interest.

ORCID iDs

Jun Guo https://orcid.org/0009-0003-4916-5156
Hengxin Sun https://orcid.org/0000-0002-2915-3006

References

[1] Shen L T, Shi Z C and Yang Z B 2019 *Entropy* **21** 917
[2] Huo M, Qin J, Cheng J, Yan Z, Qin Z, Su X, Jia X, Xie C and Peng K 2018 *Sci. Adv.* **4** eaas9401
[3] Li Z, Guo H, Liu H, Li J, Sun H, Yang R, Liu K and Gao J 2022 *Adv. Quantum Technol.* **5** 2200055

[4] van Loock P and Furusawa A 2003 *Phys. Rev.* A **67** 052315
[5] Villar A S, Martinelli M, Fabre C and Nussenzveig P 2006 *Phys. Rev. Lett.* **97** 140504
[6] Coelho A S, Barbosa F A S, Cassemiro K N, Villar A S, Martinelli M and Nussenzveig P 2009 *Science* **326** 823–6
[7] Jia X, Yan Z, Duan Z, Su X, Wang H, Xie C and Peng K 2012 *Phys. Rev. Lett.* **109** 253604
[8] Yan Z and Jia X 2015 *J. Opt. Soc. Am.* B **32** 2139
[9] Agustí A, Chang C W, Quijandría F, Johansson G, Wilson C M and Sabín C 2020 *Phys. Rev. Lett.* **125** 20502
[10] Zhai S, Yang R, Fan D, Guo J, Liu K, Zhang J and Gao J 2008 *Phys. Rev.* A **78** 14302
[11] Zhai S, Yang R, Liu K, Zhang H, Zhang J and Gao J 2009 *Opt. Express* **17** 9851–7
[12] Yang R, Zhai S, Liu K, Zhang J and Gao J 2010 *J. Opt. Soc. Am.* B **27** 2721
[13] Li T, Mitazaki R, Kasai K, Okada-Shudo Y, Watanabe M and Zhang Y 2015 *Phys. Rev.* A **91** 023833
[14] Wang H, Zheng Z, Wang Y and Jing J 2016 *Opt. Express* **24** 23459
[15] Wen J, Oh E and Du S 2010 *J. Opt. Soc. Am.* B **27** A11
[16] van Loock P and Braunstein S L 2000 *Phys. Rev. Lett.* **84** 3482–5
[17] Asavanant W *et al* 2019 *Science* **366** 373–6
[18] Wu L, Chai T, Liu Y, Zhou Y, Qin J, Yan Z and Jia X 2022 *Opt. Express* **30** 6388
[19] Liu K, Guo J, Cai C, Zhang J and Gao J 2016 *Opt. Lett.* **41** 5178
[20] Cai C, Ma L, Li J, Guo H, Liu K, Sun H, Yang R and Gao J 2018 *Photon. Res.* **6** 479
[21] Buonanno A and Chen Y 2001 *Phys. Rev.* D **64** 042006
[22] Buonanno A and Chen Y 2002 *Phys. Rev.* D **65** 042001
[23] Somiya K, Kataoka Y, Kato J, Saito N and Yano K 2016 *Phys. Lett.* A **380** 521–4
[24] Korobko M, Khalili F and Schnabel R 2018 *Phys. Lett.* A **382** 2238–44
[25] Zhang J, Sun H, Guo H, Blair C, Bossilkov V, Page M, Chen X, Gao J, Ju L and Zhao C 2023 *Appl. Phys. Lett.* **122** 261106
[26] Junker J, Wilken D, Johny N, Steinmeyer D and Heurs M 2022 *Phys. Rev. Lett.* **129** 033602
[27] Huang S and Chen A 2018 *Phys. Rev.* A **98** 063818
[28] Aggarwal N, Cullen T J, Cripe J, Cole G D, Lanza R, Libson A, Follman D, Heu P, Corbitt T and Mavalvala N 2020 *Nat. Phys.* **16** 784–8
[29] Li Y, Wang Y, Sun H, Liu K and Gao J 2023 *J. Opt.* **25** 075201
[30] Jahani S, Roy A and Marandi A 2021 *Optica* **8** 262
[31] Lugovoi V N 1979 *Physica Status Solidi* b **94** 79–86
[32] Lugiato L A, Oldano C, Fabre C, Giacobino E and Horowicz R J 1988 *Il Nuovo Cimento* D **10** 959–77
[33] Fabre C, Giacobino E, Heidmann A, Lugiato L, Reynaud S, Vadacchino M and Kaige W 1990 *Quantum Opt. J. Eur. Opt. Soc.* B **2** 159–87
[34] Kasai K, Jiangrui G and Fabre C 1997 *Europhys. Lett.* **40** 25–30
[35] Fabre C, Giacobino E, Heidmann A and Reynaud S 1989 *J. Phys.* **50** 1209–25
[36] Yu Y B, Xie Z D, Yu X Q, Li H X, Xu P, Yao H M and Zhu S N 2006 *Phys. Rev.* A **74** 042332
[37] Yu Y B, Wang H J and Feng J X 2011 *Chin. Phys. Lett.* **28** 090304
[38] Simon R 2000 *Phys. Rev. Lett.* **84** 2726–9
[39] Adesso G, Serafini A and Illuminati F 2004 *Phys. Rev.* A **70** 022318
[40] Debuisschert T, Sizmann a, Giacobino E and Fabre C 1993 *J. Opt. Soc. Am.* B **10** 1668
[41] Gardiner C W and Zoller P 2004 *Quantum Noise: A Handbook of Markovian and Non-Markovian Quantum Stochastic Methods With Applications to Quantum Optics* (Springer)
[42] Werner R F and Wolf M M 2001 *Phys. Rev. Lett.* **86** 3658–61
[43] Giedke G, Kraus B, Lewenstein M and Cirac J I 2001 *Phys. Rev.* A **64** 052303
[44] Tan A, Xie C and Peng K 2012 *Phys. Rev.* A **85** 013819
[45] Villar A, Martinelli M and Nussenzveig P 2004 *Opt. Commun.* **242** 551–63
[46] Guo J, Sun H, Liu K and Gao J 2022 *Acta Sin. Quantum Opt.* **28** 87
[47] Abraham E and Smith S D 1982 *Rep. Prog. Phys.* **45** 815–85